Crystal Structure at 2.4 Å Resolution of *Borrelia burgdorferi* Inosine 5′-Monophosphate Dehydrogenase: Evidence of a Substrate-Induced Hinged-Lid Motion by Loop 6[†,‡]

Fiona M. McMillan,[§] Marguerite Cahoon,[||] André White,[§] Lizbeth Hedstrom,[||] Gregory A. Petsko,[§] and Dagmar Ringe*[,§]

The Rosenstiel Basic Medical Sciences Research Center and Department of Biochemistry, Brandeis University, Waltham, Massachussetts 02454

Received November 16, 1999; Revised Manuscript Received January 24, 2000

ABSTRACT: The conversion of inosine 5′-monophosphate (IMP) to xanthosine 5′-monophosphate (XMP) is the committed and rate-limiting reaction in de novo guanine nucleotide biosynthesis. Inosine 5′-monophosphate dehydrogenase (IMPDH) is the enzyme that catalyzes the oxidation of IMP to XMP with the concomitant reduction of nicotinamide adenine dinucleotide (from NAD^+ to NADH). Because of its critical role in purine biosynthesis, IMPDH is a drug design target for anticancer, antiinfective, and immunosuppressive chemotherapy. We have determined the crystal structure of IMPDH from *Borrelia burgdorferi*, the bacterial spirochete that causes Lyme disease, with a sulfate ion bound in the IMP phosphate binding site. This is the first structure of IMPDH in the absence of substrate or cofactor where the active-site loop (loop 6), which contains the essential catalytic residue Cys 229, is clearly defined in the electron density. We report that a seven residue region of loop 6, including Cys229, is tilted more than 6 Å away from its position in substrate- or substrate analogue-bound structures of IMPDH, suggestive of a conformational change. The location of this loop between β6 and α6 links IMPDH to a family of β/α barrel enzymes known to utilize this loop as a functional lid during catalysis. Least-squares minimization, root-mean-square deviation analysis, and inspection of the molecular surface of the loop 6 region in the substrate-free *B. burgdorferi* IMPDH and XMP*-bound Chinese hamster IMPDH show that loop 6 follows a similar pattern of hinged rigid-body motion and indicates that IMPDH may be using loop 6 to bind and sequester substrate and to recruit an essential catalytic residue.

The rate-determining reaction in de novo guanine nucleotide biosynthesis is the conversion of inosine 5′-monophosphate (IMP)[1] to xanthosine 5′-monophosphate (XMP), which is catalyzed by inosine 5′-monophosphate dehydrogenase (IMPDH) (E.C. 1.1.1.205). Guanine nucleotides are essential to DNA synthesis, signal transduction, and cell cycle control; thus IMPDH activity is essential for cell growth and proliferation in most organisms (*1*). Human cells, for example, contain two isozymes of IMPDH with 84% sequence identity, named type I and type II (*2*). Studies have shown that type I IMPDH is constitutively expressed under normal growth conditions (*3*, *4*) whereas type II IMPDH expression is up-regulated in rapidly proliferating cells such as tumor cells or lymphocytes during an antigenic response (*2*, *3*, *5*). Specific inhibition of IMPDH impedes such increased proliferation by blocking the guanosine biosynthetic pathway (*1*). In fact, several drugs currently in clinical use for antitumor, antiviral, and immunosuppressive chemotherapy are known inhibitors of IMPDH; these drugs (and their active metabolites) are tiazofurin (TAD), ribivirin (RMP), mizoribine (MMP), and mycophenolate mofetil (MPA), respectively (*6*−*12*). Kinetic studies of IMPDH from various species reveal differences in the catalytic behavior between mammalian and bacterial IMPDHs, including variations in substrate binding and mechanism of inhibition (*13*−*17*). Such kinetic evidence suggests that variations must therefore exist in the active sites of IMPDHs, making the enzyme a potential drug design target for species-specific antiinfective chemotherapy.

The kinetic mechanisms of human type II and *Tritrichomonas foetus* IMPDH are known (*18*−*20*) (Figure 1). In both cases, substrate binding is random (*18*, *20*). In addition, it has been established in *T. foetus* IMPDH that binding of IMP occurs in two steps (*20*). The reaction begins with

[†] This work was supported by grants from the NIH (GM32415 to G.A.P. and D.R. and GM54403 to L.H.), a biophysics training grant to Brandeis University (F.M.M.), and, in part, a grant from the Lucille P. Markey Charitable Trust.

[‡] The crystal structure described in this paper has been submitted to the Brookhaven Protein Data Bank under filename 1EEP.

* Corresponding author: Sixth Floor, The Rosenstiel Basic Medical Sciences Research Center, Mail Stop 029, Brandeis University, Waltham, MA 02454. Tel (781) 736-4902; Fax (781) 736-2405; e-mail ringe@binah.cc.brandeis.edu.

[§] The Rosenstiel Basic Medical Sciences Research Center.

[||] Department of Biochemistry.

[1] Abbreviations: 6-Cl-IMP, 6-chloropurine riboside 5′-monophosphate; CBS, cystathionine β-synthase; IMP, inosine 5′-monophosphate; IMPDH, inosine 5′-monophosphate dehydrogenase; MPA, mycophenolic acid; NAD^+, nicotinamide adenine dinucleotide; NADH, reduced nicotinamide adenine dinucleotide; RMP, ribavarin monophosphate; SAD, selenazole-4-carboxamide adenine dinucleotide; TAD, β-methylene tiazofurin adenine dinucleotide; XMP, xanthosine 5′-monophosphate; XMP*, covalently bound reaction intermediate.

10.1021/bi992645l CCC: $19.00
Published on Web 03/23/2000

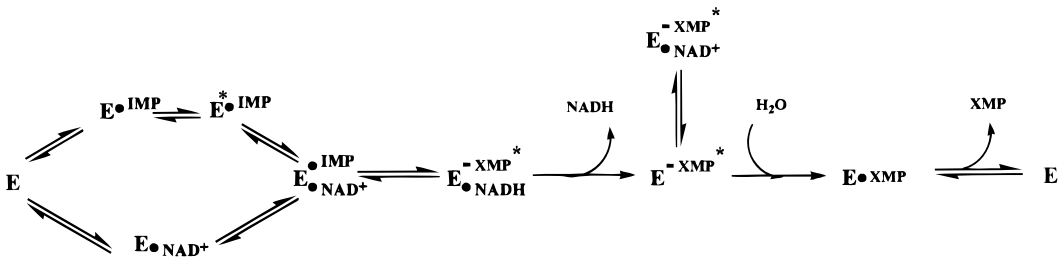

FIGURE 1: Kinetic mechanism for IMPDH from *T. foetus* (*20*).

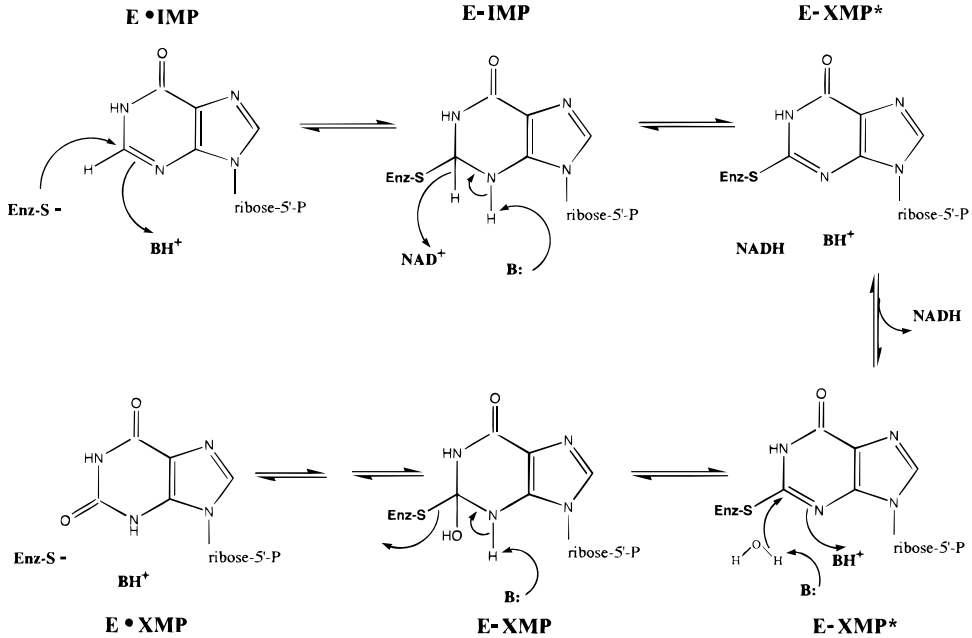

FIGURE 2: Mechanism of the IMPDH reaction. Nucleophilic attack by an active-site cysteine at the C2 position of IMP results in the formation of a covalent tetrahedral intermediate (*16*, *21*). A hydride ion is then transferred to NAD^+ (fast step) yielding NADH and a covalent E-XMP* intermediate (*22*). NADH is released and E-XMP* is irreversibly hydrolyzed (rate-limiting step) (*18*−*20*).

nucleophilic attack by an active-site cysteine-thiol at the C2 position of IMP, yielding a presumed covalent tetrahedral intermediate, E-IMP (*21*, *16*) (Figure 2). A hydride ion is then transferred from this intermediate to the B-side of the nicotinamide ring of NAD^+, giving the next reaction intermediate, E-XMP* (*22*). Hydride transfer is fast and reversible (*18*). The E-XMP* intermediate is subsequently hydrolyzed to form the product XMP in the rate-limiting step (*18*−*20*). This mechanism is similar to that of glyceraldehyde-3-phosphate dehydrogenase (GAPDH), which also involves the cysteine-mediated formation of a covalent tetrahedral intermediate (*23*). Product release is ordered, with NADH leaving before XMP hydrolysis (*18*−*20*). Presently, the structural basis of IMP binding in two steps is unclear.

IMPDH has been isolated from both mammalian and bacterial species and the three-dimensional structures of the enzymes from *T. foetus*, *Streptococcus pyogenes*, Chinese hamster, and human type II IMPDH are known (*24*−*27*). The enzymes from all of these sources have been characterized as homotetramers composed of 44−58 kDa subunits (ref *28* and references therein). The structures confirm that each monomer has an eight-stranded parallel β/α barrel fold with a 40−130 residue subdomain inserted between $\alpha 2$ and $\beta 3$ (*24*−*27*). So far, most of the structures determined for this enzyme contain a ligand bound, such as substrate, substrate analogue, product, or inhibitor. A comparison of the Chinese hamster and human type II IMPDH structures indicates that a loop containing the active-site nucleophile Cys 331 (human type II numbering) can take on different conformations (*26*, *27*). The structure of the substrate-free, sulfate-bound enzyme has been solved only for *T. foetus* IMPDH, but the active-site loop containing the catalytic cysteine is disordered in this structure (*24*). Consequently, a comparison of the conformations of the complete active sites in the presence and absence of substrate has not been possible, and currently the role of the active-site loop in the absence of substrate is unclear. It might be possible to isolate conserved structural and biochemical motifs responsible for the reaction if a structure of the enzyme in the absence of an organic ligand, but with the loop visible, were available.

IMPDH belongs to the family of enzymes possessing the triosephosphate isomerase (TIM) barrel fold (*29*). Several members of this family possess a flexible extended loop located between $\beta 6$ and $\alpha 6$ (*30*−*32*). Often referred to as loop 6, this loop is postulated to be involved in substrate binding, solvent exclusion, and/or hydrolysis of intermediates and is characterized by a large hinged, rigid-body motion, which facilitates such functions (*30*−*32*). IMPDH also possesses an extended loop 6: it is the nucleophile-containing active-site loop. Observation of characteristic loop 6 movement in IMPDH might indicate involvement in one or more of these functions as well.

We report the 2.4 Å resolution X-ray crystal structure of substrate-free IMPDH from *Borrelia burgdorferi*, the caus-

ative agent of Lyme disease (*13*, *33*). In this structure, a sulfate ion, which can be considered an analogue of phosphate, is bound in the putative IMP phosphate binding site. Excluding the subdomain, *B. burgdorferi* IMPDH has 36%, 36%, 35%, and 53% sequence identity with human type II, Chinese hamster, *T. foetus*, and *S. pyogenes* IMPDH, respectively. Overall, the structure of *B. burgdorferi* IMPDH is similar to that of other known IMPDH structures (*24*−*27*) with some important exceptions. The most striking feature is the conformation of loop 6. This loop is clearly visible in the electron density map, unlike that in the *T. foetus* SO_4^{2-}-bound IMPDH structure, and is in a different conformation than those in the substrate- and substrate analogue-bound structures. A comparison of the loop 6 conformations indicates that it is capable of large, hinged, rigid-body motion. Analysis of the active-site surface in comparison with the active sites of other known structures reveals regions of conserved electrostatic interactions even where sequence identity is low. Moreover, the active site of *B. burgdorferi* IMPDH contains some residues that appear to be conserved only among IMPDHs from bacterial species. These findings may provide a basis for the design of bacterial-specific inhibitors for use in antiinfective chemotherapy, as well as species-specific inhibitors to aid in the treatment of Lyme disease.

EXPERIMENTAL PROCEDURES

Materials. IMP, NAD^+, dithiothreitol (DTT), Trizma base, and Cibacron Blue Sepharose resin were purchased from Sigma.

Expression and Purification of B. burgdorferi IMPDH. Expression and purification of *B. burgdorferi* IMPDH was previously described in detail (*13*). The *B. burgdorferi guaB* gene was overexpressed in an IMPDH-deficient *Escherichia coli* strain and the protein was purified by affinity chromatography. The presence of active IMPDH was confirmed by a 340 nm spectrophotometric analysis of the conversion of NAD^+ to NADH in the presence of enzyme and an assay buffer of 250 μM IMP, 500 μM NAD^+, 50 mM Tris-HCl (pH 8.0), 100 mM KCl, 1 mM DTT, and 3 mM ethylenediaminetetraacetic acid (EDTA). Protein was applied to a Cibacron Blue Sepharose column (Sigma) and eluted in a linear gradient of 0−2 M KCl in 50 mM Tris-HCl (pH 8.0) and 1 mM DTT. Active eluant was applied to an IMP cross-linked affinity resin and eluted from the column in the presence of 0.5 M KCl, 50 mM Tris-HCl (pH 7.5), 1 mM DTT, and 1 mM IMP [which is approximately 30-fold greater than the K_M for IMP (29 ± 8 μM)] for *B. burgdorferi* IMPDH (*13*).

Crystallization and Data Collection. Crystals were grown at room temperature via the hanging-drop vapor-diffusion method with a 1:1 mixture of protein solution [containing 0.16 mM IMPDH, 0.5 M KCl, 50 mM Tris-HCl (pH 7.5), 1 mM DTT, 10% glycerol, and 1 mM IMP] and well solution [containing 2.2 M ammonium sulfate, poly(ethylene glycol) (PEG), 550 MME, 0.1 M Tris-HCl (pH 7.5), 10% glycerol, and 0.01 mM β-mercaptoethanol]. During crystallization there were in excess of 10^4 sulfate molecules per IMPDH monomer and the protein crystallized in the sulfate-bound form. The crystals grew to a maximum size of approximately 0.4 mm in each dimension. All X-ray data were collected and processed at the National Synchrotron Light Source at Brookhaven National Laboratories on Beamline X12B (Table 1). Crystals were flash-cooled in liquid nitrogen and the data were collected at cryogenic temperatures of approximately −180 °C (no additional cryoprotectant was needed other than that already present in the well solution). With a crystal-to-detector distance of 194.0 mm, a total of 100 frames of 90 s exposure and 1.0° oscillation were collected. A wavelength of 1.54 Å was used for the experiment. The data were processed and scaled with the programs DENZO and SCALEPACK, respectively (*34*). The crystal diffracted to approximately 2.2 Å resolution; however, data only to 2.4 Å resolution were used for refinement due to incompleteness and high *R*-merge value. The final data set, including all data, was 99% complete to 2.4 Å resolution in the space group *I*4 ($a = b = 123.28$ Å, $c = 130.11$ Å; $\alpha = \beta = \gamma = 90°$) (Table 1). There are two monomers per asymmetric unit with each monomer belonging to a separate tetrameric molecule. The symmetry axis of each tetramer is coincident with the crystallographic 4-fold *c*-axis, which is atypical.

Table 1: Statistics for *B. burgdorferi* IMPDH Data Collection and Refinement

Data Collection	
temperature	cryogenic
space group	*I*4
unit cell (Å)	
a	123.28
b	123.28
c	130.11
$\alpha = \beta = \gamma$ (deg)	90.00
resolution (Å)	2.4
total no. of reflections	255 126
no. of unique reflections	37 686 [$I/\sigma(I) > 0$]
overall $\langle I/\sigma(I)\rangle$	>14
completeness of data (%; overall/ 2.4−2.5 Å)	99.2/98.6
R-merge (%; overall[a]/2.4−2.5 Å[b])	13.1/34.3
Refinement	
resolution range (Å)	8.0−2.4
reflections used (working/free)	33 917/3767
temperature factor model	restrained group
R-factor[c]/*R*-free (%)	21.5/26.8
model used in refinement	
total non-hydrogen atoms	2343
no. of waters	57
no. of sulfate ions	1
rms deviations from ideal geometry[d]	
bond lengths (Å)	0.007
bond angles (deg)	1.42
dihedral angles (deg)	23.6
improper angles (deg)	0.86

[a] *R*-merge = $\sum|I_{obs} - I_{avg}|/\sum I_{avg}$, over all symmetry-related observations. [b] *R*-merge in the 2.49−2.40 Å shell. [c] *R*-factor = $\sum|F_{obs} - F_{calc}|/\sum F_{obs}$, over all reflections. [d] Engh and Huber parameters were used in refinement (*41*).

Molecular Replacement and Refinement. The structure was solved by the molecular replacement method using the 2.6 Å resolution structure of *T. foetus* IMPDH as a search model (coordinates were provided prior to their publication by F. Whitby and C. C. Wang) (PDB entry 1AK5; *24*) (Table 1). There was no modification to the search model, and sequence differences between *T. foetus* and *B. burgdorferi* IMPDH were later used to verify the solution. The phase problem was solved with the program package AMORE (*35*). The *T. foetus* model, which was itself incomplete, was then slightly truncated in several regions to prevent steric clashing of symmetry-generated monomers in the space group *I*4.

Otherwise, the model was unchanged, leaving the original side chains and temperature factors intact. Representing 64% of the asymmetric unit, the working 258 amino acid search model was 42% identical to the corresponding regions of *B. burgdorferi* IMPDH.

A self-rotation map of the *B. burgdorferi* data set was calculated with the program package AMORE with data from 13 to 4.0 Å. Results indicated two solutions with equivalent peaks at ($\alpha = 0.00°$, $\beta = 180.00°$, $\gamma = -31.29°$) and ($\alpha = 0.00°$, $\beta = 180.00°$, $\gamma = 58.71°$), which are clearly symmetry-related by a rotation of 90° about the crystallographic *z*-axis. With all data between 8 and 4.0 Å resolution, a 90° cross-rotation was performed with the search model but gave no clear solution. All solutions from the cross-rotation function analysis were tried during a subsequent translation step, and only one of these gave a clear translation solution with a correlation coefficient of 14.7 (the next highest correlation coefficient was 7.0). This solution was refined to ($\alpha = 87.56°$, $\beta = 77.45°$, $\gamma = 114.95°$, $t_x = 0.6800$, $t_y = 0.6667$, $t_z = 0.000$) with a correlation coefficient of 18.0 (next highest correlation was 8.1). This solution was applied to the search model as the position of the first monomer in the asymmetric unit. The position of the second monomer in the asymmetric unit was found by applying the self-rotation solution ($\alpha = 0.00°$, $\beta = 180.00°$, $\gamma = -31.29°$) to the first monomer and then performing a translation search ($t_x = 0.6866$, $t_y = 0.8288$, $t_z = 0.1351$). Refinement of the first and second monomers together showed that they have identical correlation coefficients of 18.5 and are in agreement with the self-rotation map. With this model and *B. burgdorferi* X-ray data, the initial *R*-factor for the new model after molecular replacement was 53.4%. Following a rigid-body refinement step, the *R*-factor dropped to 50.7% and electron density maps were calculated to 3.0 Å resolution from these coordinates. These first maps were of good quality, and the electron density was continuous, clear, and in agreement with the *B. burgdorferi* IMPDH sequence rather than the *T. foetus* sequence. Model rebuilding, using the program O (*36*) and with the correct amino acid sequence, gradually lowered the *R*-factor to 28.0% with an *R*-free of 34.9%. Thirty-six surface and loop side chains with disordered electron density were built in as alanines. Refinement was continued with all data to 2.4 Å resolution. Rigid-body refinement, positional refinement, simulated annealing, and grouped *B*-factor refinement were carried out initially with the X-PLOR package (*37*). The final stages of refinement were performed with the packages CNS 0.3 and CNS 0.5 (*38*). The correctness of the final model was verified with a composite simulated annealing omit map (*39*). The final model consists of 314 residues out of 404 residues in the protein. Two flexible regions of more than 40 residues each, the subdomain and the active-site flap, were highly disordered and could not be refined. Likewise, the last 14 residues of the C-terminus could not be assigned. Regions of disorder will be discussed. The final *R*-factor is 21.5% with an *R*-free of 26.5% for all reflections between 8.0 and 2.4 Å resolution. All least-squares analysis calculations were performed with the program packages O (*36*) and LSQMAN (*40*). *B. burgdorferi* IMPDH residue numbering differs from human type II IMPDH numbering due to insertions and deletions. For example, Cys 229 in *B. burgdorferi* IMPDH is analogous to the essential catalytic residue Cys 331 in human type II IMPDH.

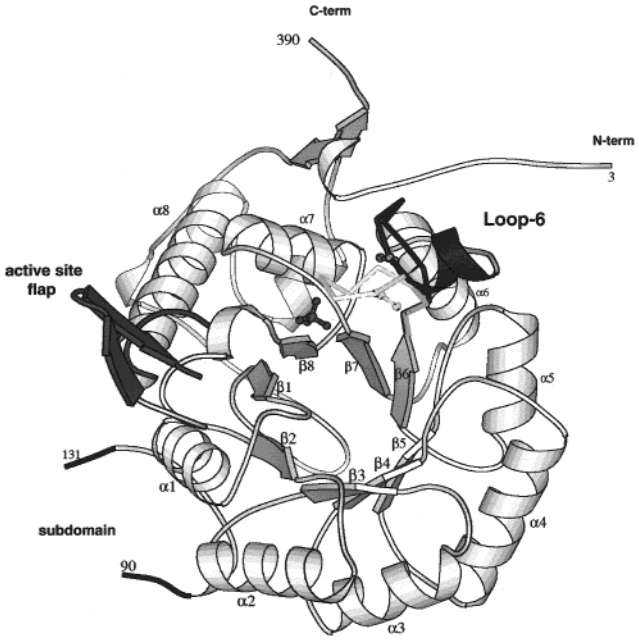

FIGURE 3: Ribbon diagram of IMPDH from *B. burgdorferi* showing secondary structure (white), including the active-site flap (gray). A sulfate molecule is bound in the IMP phosphate binding site. Located between β6 and α6, residues 224−237 form loop 6 (black), which contains the catalytic nucleophile Cys229. Superimposed upon this is the closed conformation of loop 6 as seen in Chinese hamster IMPDH (white dashed line) (*26*). This is the first view of loop 6 in the open conformation. This figure was made with Molscript v2.1 (*51*).

RESULTS AND DISCUSSION

The structure of *Borrelia burgdorferi* IMPDH was determined at 2.4 Å resolution by the molecular replacement method using the atomic coordinates for *T. foetus* IMPDH as a model (*24*). The final model comprises of 314 out of 404 amino acids and contains 57 water molecules per monomer and a sulfate ion. Regions of disorder that account for the residues missing from the model are confined to the subdomain, the active-site flap (a region distinct from loop 6), and a portion of the C-terminus. The fold of *B. burgdorferi* IMPDH is an eight-stranded β/α barrel with dimensions of 40 × 40 × 50 Å, into which is inserted a smaller, flanking subdomain of 58 amino acids between α2 and β3 (Figure 3). Excluding the subdomain, the fold of *B. burgdorferi* IMPDH is consistent with structural predictions based on primary sequence (*42*) and is similar to those of the other known IMPDHs (Figure 4), despite sequence identities ranging from only 35% to 53% (*24*−*27*). *T. foetus* IMPDH (35% sequence identity) was used as a model for molecular replacement because the *S. pyogenes* (53% sequence identity) coordinates are not available.

B. burgdorferi IMPDH is active as a homotetramer in solution (*13*) and crystallizes as such. In the crystal, the planar 4-fold axis of the tetramer is coincident with the crystallographic 4-fold axis in space group *I*4. The crystal packing of IMPDH consists of two tetramers face to face, with one rotated by 31° relative to the other so that extended flaps at the "top" of each monomer do not clash (residues 285−309). The two monomers in the asymmetric unit

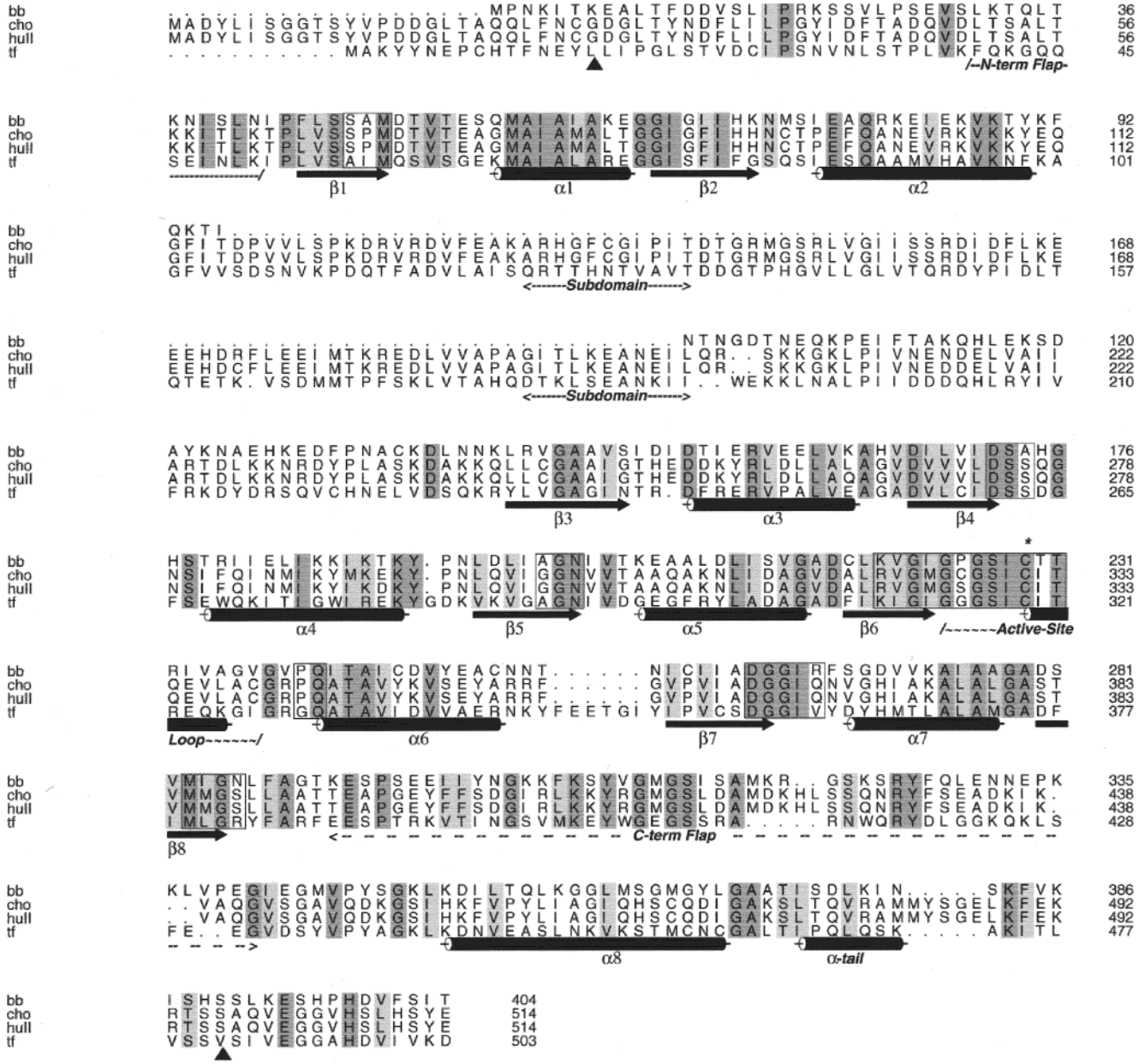

FIGURE 4: Sequence alignment of IMPDH from *B. burgdorferi*, Chinese hamster, human type II, and *T. foetus*. Overall structural alignment of these IMPDHs occurs in the region between the ▲ symbols. Shaded regions indicate the degree of sequence conservation: dark gray indicates the residues have been strictly conserved, light gray indicates residues that are homologous. Residues within the boxed regions are found in the IMP binding site of *B. burgdorferi* IMPDH. The catalytic cysteine is marked (with an asterisk). This figure was made with Alscript version 2.0 (*52*).

represent single subunits, each from an opposite corner of the facing tetramers. The observable interactions between the monomers are limited to hydrogen bonding at the flaps. Within a functional molecule, a tetramer, interactions at the subunit interfaces are primarily hydrophobic with occasional ionic interactions and include the C-terminus of one subunit interacting with the N-terminus of the other (*24*−*27*). There are additional subunit−subunit interactions that may have a specific role in catalysis. For instance, the C-terminus of one subunit comes into proximity of loop 6 from an adjacent subunit. Although unlikely to be directly involved in catalysis, it is possible that the close packing of one subunit behind the loop 6 of another could be the basis for tetramer activation via active-site stabilization (*26*).

The active site of *B. burgdorferi* IMPDH is located at the C-terminal end of the β/α barrel, consistent with all known β/α barrel enzymes, and has a similar overall topology to the active sites of known structures of IMPDH from other species (*24*−*27*), though with a few important differences. The active site comprises an IMP binding site and an NAD^+ binding site in close proximity to one another as predicted by mutagenesis, known ternary complex structures, and sequence alignment (*26*−*28*). The flexible, 13-residue loop referred to as loop 6 sits above the IMP binding site and contains the essential nucleophilic Cys 229. Also located near the active site is another flexible secondary structure element, called the active-site flap (residues 309−344). Although it has never been completely observed, it has been implicated in catalysis due to the proximity of parts of the peptide chain to the active site in crystal structures of IMPDH (*24*, *26*, *27*). For instance, in Chinese hamster IMPDH a portion of the active-site flap was observed covering the MPA-occupied

NAD^+ binding site (*26*). Therefore, we expect that the 45-residue active-site flap completes the *B. burgdorferi* NAD^+ binding pocket during catalysis. However, this extended region is also disordered in our structure. High flexibility of this flap is expected in the absence of NAD^+ and/or IMP and is consistent with a conformational change upon dinucleotide binding that is known to occur in many NAD^+ binding enzymes (*43*).

We have compared the active site architecture of IMPDH from *B. burgdorferi*, *T. foetus*, Chinese hamster, and human type II, focusing on differences due to binding states and species variation. The *B. burgdorferi* structure represents the enzyme with a sulfate bound in the phosphate binding site. The two *T. foetus* structures represent the sulfate-bound and the XMP holoenzyme (PDB entry 1AK5; *24*). The Chinese hamster structure represents the complex with MPA and the covalent E-XMP* intermediate (*26*). The human type II structure represents a ternary complex with the inhibitor SAD and an adduct of 6-Cl-IMP (PDB entry 1B30; *27*). The *S. pyogenes* structure represents the IMP bound holoenzyme (PDB entry 1ZFJ; *25*).

Substrate Binding Site. Excluding loop 6 and the active-site flap, the IMP binding site is unaffected by occupancy at the NAD^+ site. The conformation of the IMP binding has been well maintained in all of the available structures, despite the variation in sequence and ligand state. This suggests that the core structure of the IMP binding site is not greatly affected by the occupancy of the NAD^+ binding site. Most NAD^+ binding enzymes either bind substrates randomly or require NAD^+ to bind first to induce a conformational change (*43*). Kinetic studies with the human type II and *T. foetus* enzymes have shown that IMPDH follows a random binding mechanism (*18*, *20*). That the structure of the core of the IMP binding pocket is not significantly affected by the binding of other molecules in the cofactor binding site is consistent with the observation that IMP can bind either before or after NAD^+ (*18*, *20*).

There is a conserved ion-pair network in the IMP binding site. A comparison of various structures reveals that there is a conserved architecture of the IMP site with a highly conserved network of ionic interactions and hydrogen-bonding interactions. Occupancy, catalytic state, and sequence variations within the IMP binding site primarily affect the loop 6 and the active-site flap but have little effect on the conformation of the backbone or side chains that bind the phosphate and ribose of IMP. Alanine scanning studies on *E. coli* IMPDH have shown that Asp 338 is involved in IMP binding and possibly catalysis (*28*), and the analogous residue, Asp 364, was observed interacting with the ribose moiety of the E-XMP* intermediate in the Chinese hamster structure (*26*). In the *B. burgdorferi* structure, this residue (Asp 262) is in the same position. The multistructure analysis of the active site shows that Asp 262 sits at the core of a conserved ion-pair and hydrogen-bonding network (involving Lys 220, Asp 182, Asn 201, Gly 222, and Gln 241) and appears to have the additional function of stabilizing the active-site conformation (Figure 5).

A sulfate ion is bound in the IMP phosphate binding site. The location of the phosphate binding site is conserved in all IMPDH structures thus far and is found between the C-termini of β7 and β8. This site is primarily formed by a hydrogen-bonding network involving the phosphate oxygens,

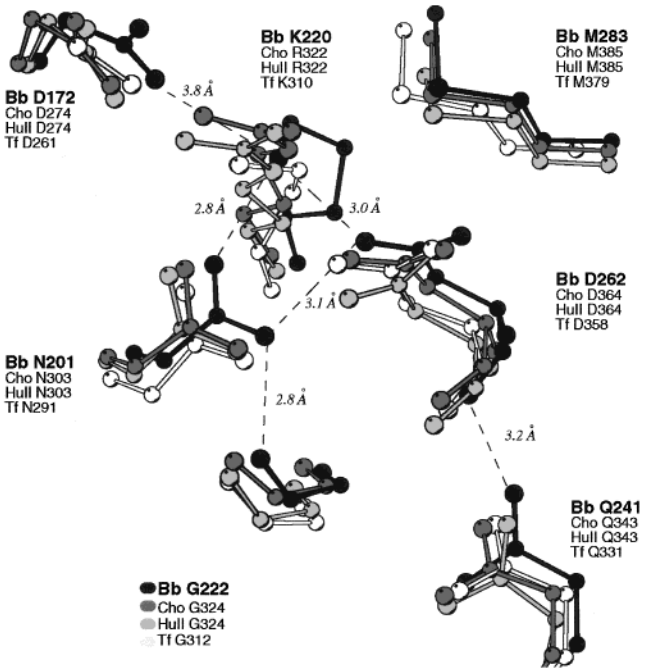

FIGURE 5: IMPDHs from *B. burgdorferi* (Bb; black), Chinese hamster (Cho; dark gray), human type II (HuII; light gray), and *T. foetus* (Tf; white) were aligned on the basis of all common secondary structural elements excluding loop 6 and the active-site flap (*24*, *26*, *27*). Viewed here in detail, the IMP binding site reveals a highly conserved internal architecture. The bottom of the IMP binding site is stabilized by a network of ion pairs and hydrogen bonds involving several highly conserved amino acids. Bond distances are given for the residue interactions in the *B. burgdorferi* IMPDH structure. Each amino acid is identified by the sequence number as it occurs in the individual enzyme. Note that residue K220 of Bb can be either an arginine or a lysine; however, the functionality is conserved. This figure was made with Molscript v2.1 (*51*).

backbone amide groups, and fixed water molecules (*24*−*27*). In *B. burgdorferi* IMPDH, participants in this network include Asp 262 (through a water molecule) and the backbone amide groups of Gly 264, Gly 285, and Asn 286. The active-site flap, which is disordered in *B. burgdorferi* IMPDH, closes over the active site upon NAD^+ binding and contributes the hydroxyl of Tyr 411 to the phosphate binding site in the structure from Chinese hamster IMPDH (*26*). This tyrosine is conserved in all IMPDHs and is expected to have the same function in *B. burgdorferi*. The Chinese hamster and human type II structures of IMPDH show that the phosphate binding site is completed by a highly conserved serine from the closed loop 6, indicating a possible relationship between phosphate binding and loop 6 closure (*26*, *27*). The structural conservation of this site and its high selectivity and affinity for phosphate (or phosphate analogues such as sulfate) may help guide the specific binding of IMP and its analogues and should be considered in the design of tight-binding inhibitors.

Loop 6. The known structures of IMPDH contain an extended loop between β6 and α6 of the barrel (*24*−*27*). This loop 6 is 13 residues long and includes a short α-helix immediately following the catalytic cysteine. Sequence identity across species is quite high in this region (Figure 6), indicating this motif has been conserved across all IMPDHs. In both the Chinese hamster and human type II structures, the loop covers the bound ligand, although the

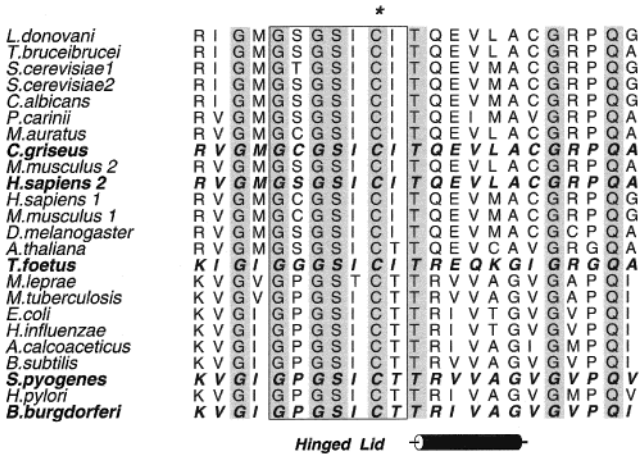

FIGURE 6: Sequence alignment of the active-site loop, loop 6. Boldface type indicates that the structure of IMPDH from that species has been solved. Shaded regions indicate 100% sequence identity across all species. On the basis of current structural information, the boxed region shows which residues comprise the mobile hinged lid of loop 6. This figure was made with Alscript version 2.0 (52).

helix in the human type II structure adopts a more extended conformation as compared with the Chinese hamster structure, to accommodate the covalently bound inhibitor 6-Cl-IMP (*26*, *27*). The particularly glycine-rich loop 6 of *T. foetus* IMPDH was disordered in both the sulfate- and the XMP-bound structures, implying that this loop is highly flexible in these binding states (*24*).

Loop 6 is well-ordered in the *B. burgdorferi* IMPDH structure. Our molecular replacement model was truncated in this region; as a result the observed loop in *B. burgdorferi* IMPDH is devoid of model bias. Moreover, a simulated annealing omit map of this region reveals electron density features that are unambiguous (Figure 7). The orientation of loop 6 in the *B. burgdorferi* sulfate-bound enzyme is quite different from that of the loops in any of the ternary-complex structures. Although the position of the short helix of the *B. burgdorferi* loop 6 is quite similar to that in the Chinese hamster structure, the first seven residues of the loop, including the catalytic cysteine, are turned back into an open conformation. As a result, the IMP binding site is fully exposed to solvent and the cysteine is oriented such that, were it to remain there, IMP could not bind in its known position (*24*−*27*) and still be susceptible to nucleophilic attack by Cys 229. Superposition of the α-carbons of the first seven residues of the Chinese hamster IMPDH loop 6 on those from *B. burgdorferi* IMPDH reveals a nearly identical backbone shape and strongly suggests that these residues move together as a rigid body. We propose that loop 6 functions as a hinged rigid-body lid that covers the active site upon substrate binding. A comparison of IMPDH with other β/α barrel enzymes containing functional β6 loops indicates that this type of conformational change is common to all of them.

There is a loop 6 motif in several β/α barrel enzymes. An extended flexible loop covering the active site has been observed following β-strand 6 in the eight-stranded β/α barrel enzymes triosephosphate isomerase (TIM), tryptophan synthase (α subunit) (TSα), phosphoribosyl anthranilate isomerase, and ribulose bisphosphate carboxylase (Rubisco) among others (*30*−*32*, *44*−*47*). Structural and biochemical data have shown that this loop undergoes a conformational change from an open to a closed position upon ligand binding in both TIM and TSα (*30*, *31*, *44*). In TIM, loop 6 moves approximately 7 Å as a hinged rigid body, such that the internal loop structure is virtually identical in the open and closed positions (*31*). Moreover, high sequence identity across species for the loop region suggests that this hinged lid movement occurs in all TIMs (*31*). In these lid-containing β/α barrel enzymes, it is postulated that loop closure sequesters the substrate from solvent as well as prevents the premature release of catalytic intermediates, thus creating a more controlled environment for the catalytic reaction to take place (*30*, *31*, *44*, *45*).

Loop 6 of *B. burgdorferi* IMPDH moves as a rigid body. The structures of *B. burgdorferi* and Chinese hamster IMPDHs were compared in order to determine whether loop 6 moves as a rigid body. The structures were truncated to include only the β/α barrel core and loop 6 and were subsequently superimposed by least-squares optimization (*40*). Although Chinese hamster and *B. burgdorferi* IMPDH

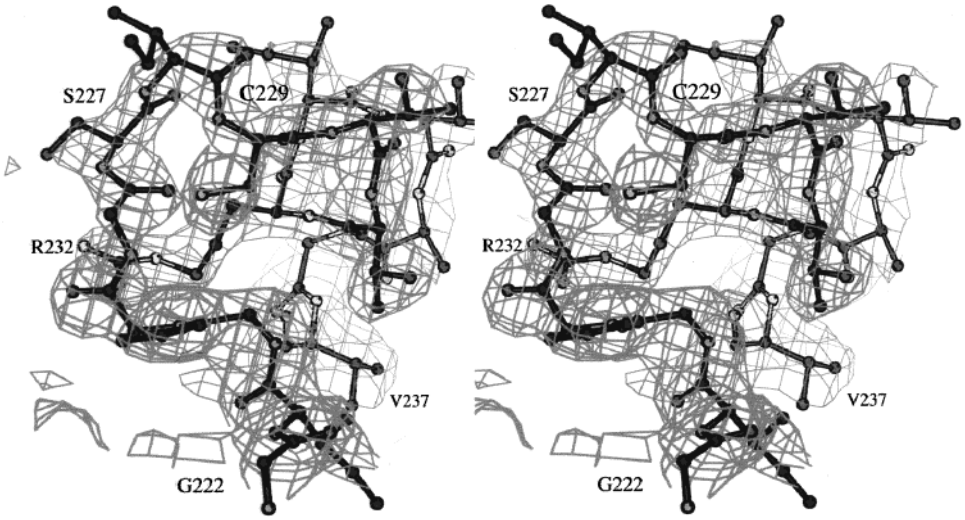

FIGURE 7: Electron density map of loop 6: stereoview of a simulated annealing omit map with coefficients $2F_o - F_c$ calculated at 2.4 Å resolution. This map clearly shows the continuity of the electron density of loop 6 in its open conformation. This figure was made with Molscript v2.1 (*51*).

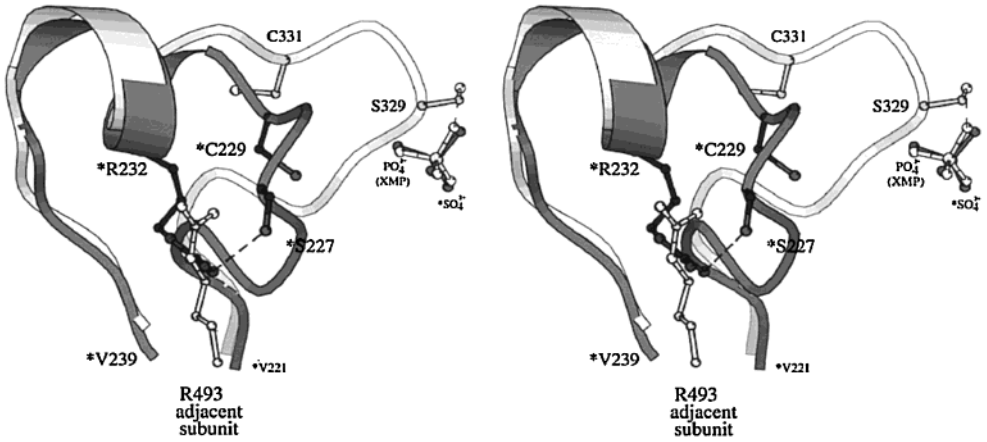

FIGURE 8: Stereoview of the conformations of loop 6 from the structures of *B. burgdorferi* (Bb; *) and Chinese hamster (Cho) IMPDH (*26*). This loop is in the closed conformation in Cho, and in the open conformation in Bb. The consequence of this difference is that the active-site cysteines (229_{Bb} and 331_{Cho}) are 3.7 Å apart. The corresponding serines 227_{Bb} and 329_{Cho} are over 10 Å apart, and 227_{Bb} is stabilized by an interaction with Arg 232_{Bb}. Arg 232_{Bb} is not conserved in Chinese hamster; however, Arg 493_{Cho} from an adjacent subunit compensates for this. The bound sulfate molecule in the *B. burgdorferi* structure clearly binds in the same location as the phosphate moiety of XMP* in the Chinese hamster structure. This figure was made with Molscript v2.1 (*51*).

Table 2: Agreement between Superimposed Cα Atoms from *B. burgdorferi* and Chinese Hamster IMPDH

	α/β barrel only[a,b] (barrel lsq)	loop 6 only[a,c] (barrel lsq)	loop 6 only[a,c,d] (loop lsq)
RMSD (Å)	1.2	6.1	1.1
maximum distance (Å)	4.2	10.1	na

[a] Corresponding Cα atoms are compared. [b] Loop 6 was omitted from calculations. [c] α/β barrel was omitted from calculations. [d] Just residues 326−332 from Chinese hamster loop 6 were superimposed onto residues 224−230 from *B. burgdorferi* loop 6 by least-squares analysis.

only share 35% sequence identity, the β/α cores overlap quite well, with a root-mean-square deviation (RMSD) of corresponding Cα atoms of less than 1.2 Å. In contrast, the corresponding main chain atoms of the seven shifted loop 6 residues have an RMSD of more than 6 Å (Table 2). In particular, the Cα of Ser 227 in *B. burgdorferi* IMPDH is over 10 Å away from its position in the Chinese hamster ternary complex (Figure 8). A comparison of the positional differences in the corresponding Cα atoms across both the β/α barrel and loop 6 shows that gross conformational differences are localized in the loop 6 region only. These differences are not accounted for by species specific differences alone, especially when considering that the loop 6 region has much higher sequence identity among all IMPDHs than does the rest of the enzyme. When just the loop 6 fragments from *B. burgdorferi* and Chinese hamster IMPDHs were superimposed, their conformations were almost identical, with an RMSD on α-carbons of only 1.1 Å (Figure 9). This result shows that the internal structure of loop 6 has remained intact and that the loop most likely moves as a rigid body. This behavior is very similar to that of loop 6 in TIM and Rubisco (*31*, *32*). The effect of loop closure is best demonstrated by a comparison of the solvent accessible surface area of the IMP sites from open and closed structures, which shows that the open conformation is considerably more solvent-accessible than the closed conformation.

In *B. burgdorferi* IMPDH, Ser 227 appears to be involved in the hinged-lid mechanism of loop 6. The analogous residue, Ser 329, is observed interacting with the phosphate of the ligand in both the Chinese hamster and human type

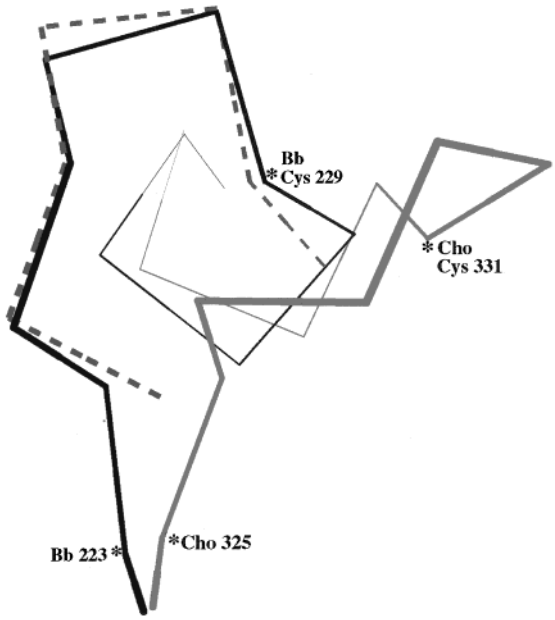

FIGURE 9: Conformation of the flexible region of loop 6 for *B. burgdorferi* IMPDH (solid black line) was compared to that of Chinese hamster IMPDH (solid gray line). When the α-carbon chain of seven loop 6 residues from Chinese hamster IMPDH (*26*) are superimposed upon the corresponding α-carbons in *B. burgdorferi* IMPDH by least-squares minimization (dashed gray line), the mobile loop maintains a fixed internal structure, indicating that loop 6 moves as a rigid body.

II structures (*26*, *27*), at an OH_{serine} to $O^-_{phosphate}$ distance of 2.8 and 2.5 Å, respectively. However, in the open conformation seen in sulfate-bound *B. burgdorferi* IMPDH, the hydroxyl of Ser 227 is more than 13 Å from the sulfate ion. A proline at position 225, which is conserved only among bacterial forms of the enzyme (Figure 6), is not responsible for the position of loop 6 in this structure. *S. pyogenes* IMPDH also contains a proline at this position; recently the structure of IMP-bound *S. pyogenes* IMPDH was solved, and an OH_{serine} to $O^-_{phosphate}$ distance of 2.8 Å was reported (*25*). This suggests that loop 6 is closed in this structure, allowing Ser 227 (*B. burgdorferi* numbering) to interact with the phosphate moiety of IMP. The open position of loop 6

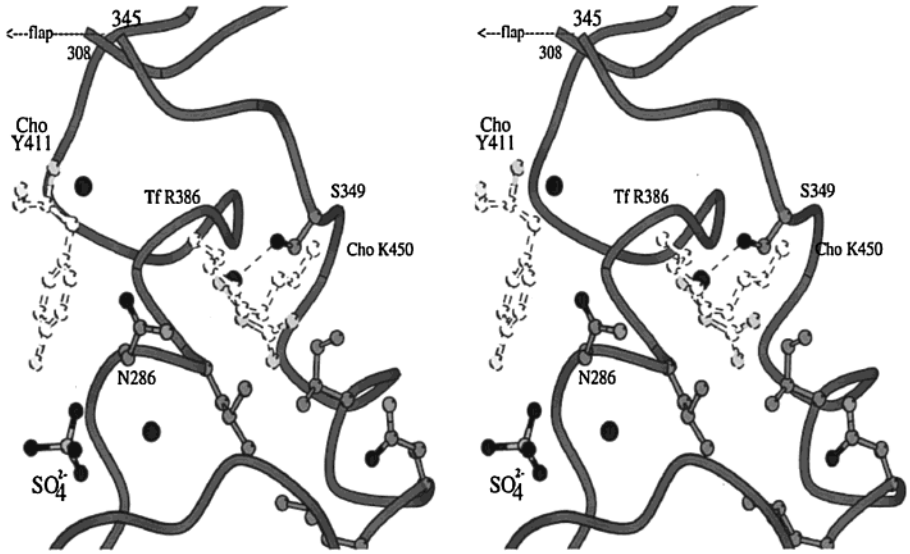

FIGURE 10: Stereoview of a novel solvent pocket. Ser349 from *B. burgdorferi* IMPDH is a lysine or an arginine in all other species including Chinese hamster (K450), with the exception of *T. foetus* (A440) (*24*, *26*). However, *T. foetus* IMPDH compensates with Arg386 (glycine in all other species), which occupies an analogous position (*24*). Thus, only *B. burgdorferi* IMPDH contains a small hydrophilic residue at position 349, creating a novel solvent binding site within proximity of both the phosphate binding site and the beginning of the flexible active-site flap. The position of the conserved flap residue Tyr 411 from the Chinese hamster structure during flap closure is also shown (*26*). This figure was made with Molscript v2.1 (*51*).

appears to be stabilized by an interaction between Ser 227 and Arg 232 (Figure 8). This arginine is not conserved at position 232 in all IMPDHs; however, in every species that does not contain an arginine at this position, a replacement arginine has appeared at the C-terminus of an adjacent subunit, such that the position of the functional group of arginine has been conserved. It is possible that Ser 227, which is conserved in all IMPDHs, is part of a mechanism for loop closure upon substrate binding. In the case of TIM, which binds D-glyceraldehyde 3-phosphate, it has been observed that closure of the loop analogous to loop 6 in IMPDH allows new hydrogen bonds to form between the phosphate and the mobile loop, presumably contributing to tight binding (*44*). Furthermore, it is interesting to note that the binding of a sulfate molecule does not induce loop closure in TIM (*48*).

Unique Solvent Binding Site Near the Active-Site Flap. *B. burgdorferi* IMPDH has very few residues that are unique in the region of the active site for purposes of species-specific inhibition. However, Ser 349 is located in proximity to the phosphate binding site and is an Arg or Lys in all other species, including Chinese hamster (Lys 450) with one exception: in *T. foetus* IMPDH it is an alanine. In *B. burgdorferi* IMPDH, Gly 290 sits nearby Ser 349. A glycine is conserved at this position in all species except one: in *T. foetus*, it is an arginine. The functional group of this arginine (R386) in *T. foetus* occupies the same place as the functional group of Lys 450 in Chinese hamster (Figure 10). In *B. burgdorferi* IMPDH, a water molecule that is hydrogen-bonded to Ser 349 occupies this space. This solvent pocket is both accessible to and capable of binding a solvent molecule and is in a position to affect the beginning of the active-site flap. Consequently, it could be considered as a potential chelation site for the design of inhibitors that target the phosphate binding site or hope to block the closing of the active-site flap.

Conclusion. IMPDH catalyzes the rate-limiting and concomitant step in de novo guanine nucleotide biosynthesis and is therefore an important enzyme for DNA production, cell cycle regulation, and cell proliferation. Inhibitors of IMPDH are already used in anticancer chemotherapy, and their use as immunosuppressants following organ transplants is common (*6*−*12*). However, current inhibitors in clinical use can have toxic side effects (*49*, *50*). The development of highly effective, nontoxic (and perhaps infection-specific) inhibitors will require a thorough understanding of the structure and function of IMPDH. The structure of sulfate-bound *B. burgdorferi* IMPDH allows us to view the conformation of loop 6 in the substrate-free state for the first time. A comparison with other structures of IMPDH has yielded several observations about how the enzyme controls the environment of the active site. A conserved ion-pair network at the core of the IMP binding site allows a consistent internal architecture in this region, regardless of the catalytic state. With the functional groups in the IMP pocket fixed in place, IMPDH employs flexible secondary structural elements to bind substrate and complete the active site. The large active-site flap has been known to close down upon the NAD^+ site during catalysis (and to partially cover the IMP site as well) (*26*, *27*). However, the structure of *B. burgdorferi* IMPDH shows that this is unlikely to be the only substantial conformational change that occurs upon substrate binding. Loop 6 in *B. burgdorferi* IMPDH is found in an open position, exposing the IMP binding site to both solvent and incoming substrate. The location of this loop between β6 and α6 links IMPDH to a family of eight-stranded β/α barrel enzymes known to utilize this loop as a functional lid during catalysis. Least-squares minimization and RMSD analysis of loop 6 in the sulfate-bound *B. burgdorferi* IMPDH and XMP*-bound Chinese hamster IMPDH show that loop 6 follows a similar pattern of hinged, rigid-body motion and implies that IMPDH may be using loop 6 to bind and sequester substrate and to recruit the catalytic residue Cys 229. The residues that make up loop 6 in *B. burgdorferi* IMPDH are strictly conserved in all bacterial forms of the enzyme and are 98% identical to mammalian IMPDHs. Ser

227, which is conserved in all known IMPDHs, appears to have a role in stabilizing both the open and closed forms of loop 6. The open form of the enzyme may serve as a template for the development of inhibitors that trap the enzyme in this position, thereby preventing catalysis. Moreover, the structure of the open enzyme may also identify novel inhibitor binding sites.

ACKNOWLEDGMENT

We thank Tracy Arakaki for assistance in data collection. We also thank Jennifer A. Digits and Barry M. Goldstein for helpful discussions.

REFERENCES

1. Weber, G. (1983) *Cancer Res. 43*, 3466−3492.
2. Natsumeda, Y., Ohno, S., Kawasaki, H., Konno, Y., Weber, G., and Suzuki, K. (1990) *J. Biol. Chem. 265*, 5292−5295.
3. Nagai, M., Natsumeda, Y., and Weber, G. (1992) *Cancer Res. 52*, 258−261.
4. Konno, Y., Natsumeda, Y., Nagai, M., Yamaji, Y., Ohno, S., Suzuki, K., and Weber, G. (1991) *J. Biol. Chem. 266*, 506−509.
5. Nagai, M., Natsumeda, Y., Konno, Y., Hoffman, R., Irino, S., and Weber, G. (1991) *Cancer Res. 51*, 3886−3890.
6. Cooney, D., Jayaram, H., Gebeyehu, G., Betts, C., Kelley, J., Marquez, V., and Johns, D. (1982) *Biochem. Pharmacol. 31*, 2133−2136.
7. Smith, C., Fontenelle, L., Muzik, H., Paterson, A., Unger, H., Brox, L., and Henderson, J. (1974) *Biochem. Pharmacol. 23*, 2727−2735.
8. Franklin, T., and Cook, J. (1969) *Biochem. J. 113*, 515−524.
9. Streeter, D. G., Witkowski, J. T., Khare, G. P., Sidwell, R. W., Bauer, R. J., Robins, R. K., and Simon, L. N. (1973) *Proc. Natl. Acad. Sci. U.S.A. 70*, 1184−1188.
10. Franklin, T., and Morris, W. P. (1994) *Adv. Enzyme Regul. 34*, 107−118.
11. Koyama, H., and Tsuji, M. (1983) *Biochem. Pharmacol. 32*, 3547−3553.
12. Allison, A. C. (1993) *Immunol. Rev. 136*, 5−28.
13. Zhou, X., Cahoon, M., Rosa, P., and Hedstrom, L. (1997) *J. Biol. Chem. 272*, 21977−21981.
14. Hupe, D. J., Azzolina, B. A., and Behrens, N. D. (1986) *J. Biol. Chem. 261*, 8363−8369.
15. Wang, W., Papov, V. V., Minakawa, N., Matsuda, A., Biemann, K., and Hedstrom, L. (1996) *Biochemistry 35*, 95−101.
16. Verham, R., Meek, T. D., Hedstrom, L., and Wang, C. C. (1987) *Mol. Biochem. Parasitol. 24*, 1−12.
17. Huete-Perez, J. A., Wu, J. C., Whitby, F. G., and Wang, C. C. (1995) *Biochemistry 34*, 13889−13894.
18. Wang, W., and Hedstrom, L. (1997) *Biochemistry 36*, 8479−8483.
19. Xiang, B., and Markham, G. D. (1997) *Arch. Biochem. Biophys. 348*, 378−382.
20. Digits, J. A., and Hedstrom, L. (1999) *Biochemistry 38*, 2695−2306.
21. Link, J. O., and Straub, K. (1996) *J. Am. Chem. Soc. 118*, 2091−2092.
22. Cooney, D., Hamel, E., Cohen, M., Kang, G. J., Dalal, M., and Marquez, V. (1987) *Biochim. Biophys. Acta 916*, 89−93.
23. Harris, J. I., and Waters, M. (1976) *Enzymes (3rd Ed.) 13*, 1−49.
24. Whitby, F. G., Luecke, H., Kuhn, P., Somoza, J. R., Huete-Perez, J. A., Phillips, J. D., Hill, C. P., Fletterick, R. J., and Wang, C. C. (1997) *Biochemistry 36*, 10666−10674.
25. Zhang, R., Evans, G., Rotella, F. J., Westbrook, E. M., Beno, D., Huberman, E., Joachimiak, A., and Collart, F. R. (1999) *Biochemistry 38*, 4691−4700.
26. Sintchak, M. D., Fleming, M. A., Futer, O., Raybuck, S. A., Chambers, S. P., Caron, P. R., Murcko, M., and Wilson, K. P. (1996) *Cell 85*, 921−930.
27. Colby, T. D., Vanderveen, K., Strickler, M. D., Markham, G. D., and Goldstein, B. M. (1999) *Proc. Natl. Acad. Sci. U.S.A. 96*, 3531−3536.
28. Kerr, K. M. (1997) Doctoral Thesis, Department of Biochemistry, Brandeis University, Waltham, MA.
29. Farber, G. K., and Petsko, G. A. (1990) *Trends Biochem. Sci. 15*, 268−234.
30. Brzovic, P. S., Hyde, C. C., Miles, E. W., and Dunn, M. F. (1993) *Biochemistry 32*, 10404−10413.
31. Joseph, D., Petsko, G. A., and Karplus, M. (1990) *Science 249*, 1425−1428.
32. Lundqvist, T., and Schneider, G. (1991) *J. Biol. Chem. 266*, 12604−12611.
33. Burgdorfer, W., Barbour, A. G., Hayes, S. F., Benach, J. L., Grunwaldt, E., and Davis, J. P. (1982) *Science 216*, 1318−1319.
34. Otwinowski, Z., (1993) Oscillation Data Reduction Program, in *Data Reduction and Processing*, Proceedings of the CCP4 Study Weekend, 29−30 January, 1993, (Sawyer, L., Issacs, N., and Bailey, S., Eds.) pp 56−62, SERC Daresbury Laboratory, Warrington, England.
35. Navaza, J. (1994) *Acta Crystallogr. A50*, 157−163.
36. Jones, T. A., Zou, J. Y., Cowan, S. W., and Kjeldgaard, M. (1991) *Acta Crystallogr. A47*, 110−119.
37. Brunger, A. T. (1992) *X-PLOR: A System for X-ray Crystallography and NMR*, The Howard Hughes Medical Institute and the Department of Molecular Biophysics and Biochemistry, Yale University, New Haven, CT.
38. Brunger, A. T., Adams, P. D., Clore, G. M., Delano, W. L., Gros, P., Grosse-Kunstleve, R. W., Jiang, J.-S., Kuszewski, J., Nilges, M., Pannu, N. S., Read, R. J., Rice, L. M., Simonson, T., and Warren, G. L. (1998) *Acta Crystallogr. D54*, 905−921.
39. Hodel, A., Kim, S. H., and Brunger, A. T. (1992) *Acta Crystallogr. A48*, 851−858.
40. Kleygwegt, G. J., and Jones, T. A. (1997) *Methods Enzymol. 277*, 525−545.
41. Engh, R. A., and Huber, R. (1991) *Acta Crystallogr. A47*, 392−399.
42. Bork, P., Gellerich, J., Groth, H., Hooft, R., and Martin, F. (1995) *Protein Sci. 4*, 268−274.
43. Bellamacina, C. R. (1996) *FASEB J. 10*, 1257−1269.
44. Pompliano, D. L., Peyman, A., and Knowles, J. R. (1990) *Biochemistry 29*, 3186−3194.
45. Rhee, S., Parris, K. D., Hyde, C. C., Ahmed, S. A., Miles, E. W., and Davies, D. R. (1997) *Biochemistry 36*, 7664−7680.
46. Brzovic, P. S., Sawa, Y., Hyde, C. C., Miles, E. W., and Dunn, M. F. (1992) *J. Biol. Chem. 267*, 13028−13088.
47. Priestle, J. P.; Grutter, M. G., White, J. L., Vincent, M. G., Kania, M., Wilson, E., Jardetzky, T. S., Kirschner, K., and Jansonius, J. N. (1987) *Proc. Natl. Acad. Sci. U.S.A. 87*, 5690−5694.
48. Noble, M. E., Zeelen, J. P., and Wierenga, R. K. (1993) *Proteins: Struct., Funct., Genet. 16*, 311−326.
49. Gruessner, R. W., Sutherland, D. E., Drangstveit, M. B., Wrenshall, L., Humar, A., and Gruessner, A. C. (1998) *Transplantation 66*, 318−323.
50. Pirsch, J. D., and Sollinger, H. W. (1996) *Ther. Drug Monit. 18*, 357−361.
51. Kraulis, P. J. (1991) *J. Appl. Crystallogr. 24*, 946−950.
52. Barton, G. J. (1993) *Protein Eng. 6*, 37−40.

BI992645L